Visible light communication using InGaN optical sources with AlInGaP nanomembrane down-converters

J. M. M. Santos[1,*], S. Rajbhandari[2], D. Tsonev[3], H. Chun[2], B. Guilhabert[1], A. Krysa[4], A. E. Kelly[5], H. Haas[3], D. C. O'Brien[2], N. Laurand[1] and M. D. Dawson[1]

[1]*Institute of Photonics, Department of Physics, SUPA, University of Strathclyde, Glasgow, UK*
[2]*Department of Engineering Science, University of Oxford, Oxford, UK*
[3]*Li-Fi R&D Centre, Institute for Digital Communications, University of Edinburgh, Edinburgh, UK*
[4]*Electronic & Electrical Engineering, University of Sheffield, Sheffield, UK*
[5]*Electronic & Electrical Engineering, University of Glasgow, Glasgow, UK*
[*]*joao.santos@strath.ac.uk*

Abstract: We report free space visible light communication using InGaN sources, micro-LEDs and a laser diode, down-converted by a red-emitting AlInGaP multi-quantum-well nanomembrane. In the case of micro-LEDs, the AlInGaP nanomembrane is capillary-bonded between the sapphire window of a micro-LED array and a hemispherical sapphire lens for a truly integrated optical source. The sapphire lens improves the extraction efficiency of the color-converted light. For the case of the down-converted laser diode, one side of the nanomembrane is bonded to a sapphire lens and the other side optionally onto a reflector; this nanomembrane-lens structure is remotely excited by the laser diode. Data transmission up to 867 Mb/s using PAM and OFDM modulation schemes is demonstrated for the micro-LED-integrated nanomembrane. A data rate of 1.2Gb/s is achieved using orthogonal frequency division modulation (ODFM) with the laser diode pumped sample.

OCIS codes: (000.0000) General; (000.2700) General science.

References and links

1. S. Nakamura and M. R. Krames, "History of gallium-nitride-based light-emitting diodes for illumination," Proc. IEEE **101**, 2211–2220 (2013).
2. H. Masui, J. S. Speck, and S. P. Denbaars, "Non-polar-oriented InGaN light-emitting diodes for liquid-crystal-display backlighting," J. Soc. Inf. Disp. **16**, 571–578 (2012).
3. G. Corbellini, K. Aksit, S. Schmid, S. Mangold, and T. R. Gross, "Connecting Networks of Toys and Smartphones with Visible Light Communication," IEEE Commun. Mag. 72–78 (2014).
4. J. J. Wierer, J. Y. Tsao, and D. S. Sizov, "Comparison between blue lasers and light-emitting diodes for future solid-state lighting," Laser Photonics Rev. **993**, 963–993 (2013).
5. C. W. Chow, C. H. Yeh, Y. Liu, and Y. F. Liu, "Digital Signal Processing for Light Emitting Diode Based Visible Light Communication," IEEE Photonics Soc. Newletter 9–13 (2012).
6. M. R. Krames, O. B. Shchekin, R. Müller-Mach, G. O. Müller, L. Zhou, G. Harbers, and M. G. Craford, "Status and Future of High-Power Light-Emitting Diodes for Solid-State Lighting," J. Disp. Technol. **3**, 160–175 (2007).
7. M. S. Shur and A. Žukauskas, "Solid-state lighting: Toward superior illumination," Proc. IEEE **93**, 1691–1703 (2005).
8. J. Herrnsdorf, B. Guilhabert, J. J. D. McKendry, Z. Gong, D. Massoubre, S. Zhang, S. Watson, A. E. Kelly, E. Gu, N. Laurand, and M. D. Dawson, "Hybrid organic/GaN photonic crystal light-emitting diode," Appl. Phys. Lett. **101**, 141122 (2012).
9. M. T. Sajjad, P. P. Manousiadis, H. Chun, D. A. Vithanage, S. Rajbhandari, A. L. Kanibolotsky, G. Faulkner, D. O'Brien, P. J. Skabara, I. D. W. Samuel, and G. A. Turnbull, "Novel Fast Color-Converter for Visible Light Communication Using a Blend of Conjugated Polymers," ACS Photonics **2**, 150203083931000 (2015).

10. N. Laurand, B. Guilhabert, J. McKendry, A. E. Kelly, B. Rae, D. Massoubre, Z. Gong, E. Gu, R. Henderson, and M. D. Dawson, "Colloidal quantum dot nanocomposites for visible wavelength conversion of modulated optical signals," Opt. Mater. Express **2**, 250 (2012).
11. D. Schiavon, M. Binder, A. Loeffler, and M. Peter, "Optically pumped GaInN / GaN multiple quantum wells for the realization of efficient green light-emitting devices Optically pumped GaInN / GaN multiple quantum wells for the realization of efficient green light-emitting devices," **113509**, (2013).
12. J. M. M. Santos, B. E. Jones, P. J. Schlosser, S. Watson, J. Herrnsdorf, B. Guilhabert, J. J. D. McKendry, J. De Jesus, T. a Garcia, M. C. Tamargo, A. E. Kelly, J. E. Hastie, N. Laurand, and M. D. Dawson, "Hybrid GaN LED with capillary-bonded II–VI MQW color-converting membrane for visible light communications," Semicond. Sci. Technol. **30**, 035012 (2015).
13. M. A. Haase, J. Xie, T. A. Ballen, J. Zhang, B. Hao, Z. H. Yang, T. J. Miller, X. Sun, T. L. Smith, and C. A. Leatherdale, "II–VI semiconductor color converters for efficient green, yellow, and red light emitting diodes," Appl. Phys. Lett. **96**, 231116 (2010).
14. J. J. D. McKendry, R. P. Green, A. E. Kelly, Z. Gong, B. Guilhabert, D. Massoubre, E. Gu, and M. D. Dawson, "High-Speed Visible Light Communications Using Individual Pixels in a Micro Light-Emitting Diode Array," IEEE Photonics Technol. Lett. **22**, 1346–1348 (2010).
15. Z. L. Liau, "Semiconductor wafer bonding via liquid capillarity," Appl. Phys. Lett. **77**, 651 (2000).
16. Z. Gong, S. Jin, Y. Chen, J. McKendry, D. Massoubre, I. M. Watson, E. Gu, and M. D. Dawson, "Size-dependent light output, spectral shift, and self-heating of 400 nm InGaN light-emitting diodes," J. Appl. Phys. **107**, 013103 (2010).
17. N. Laurand, J. McKendry, B. Guilhabert, a. E. Kelly, B. Rae, R. Henderson, D. Massoubre, Z. Gong, E. Gu, and M. D. Dawson, "Hybrid organic/inorganic nanocrystal-based composite for color-conversion and visible light communications," 2010 IEEE Photinic Soc. 23rd Annu. Meet. 150–151 (2010).
18. D. O'Brien, R. Turnbull, H. Le Minh, G. Faulkner, O. Bouchet, P. Porcon, M. El Tabach, E. Gueutier, M. Wolf, and L. Grobe, "High-Speed Optical Wireless Demonstrators: Conclusions and Future Directions," J. Light. Technol. **30**, 2181–2187 (2012).
19. D. Tsonev, H. Chun, S. Rajbhandari, J. J. D. Mckendry, S. Videv, E. Gu, M. Haji, S. Watson, A. E. Kelly, G. Faulkner, M. D. Dawson, H. Haas, and D. O. Brien, "A 3-Gb / s Single-LED OFDM-Based Wireless VLC Link Using a Gallium Nitride μLED," IEEE Photonics Soc. Newletter **26**, 637–640 (2014).
20. Y. C. Shen, G. O. Mueller, S. Watanabe, N. F. Gardner, a. Munkholm, and M. R. Krames, "Auger recombination in InGaN measured by photoluminescence," Appl. Phys. Lett. **91**, 37–40 (2007).
21. J. Hader, J. V. Moloney, B. Pasenow, S. W. Koch, M. Sabathil, N. Linder, and S. Lutgen, "On the importance of radiative and Auger losses in GaN-based quantum wells," Appl. Phys. Lett. **92**, 261103 (2008).
22. E. F. Schubert, *Light-Emitting Diodes*, 2nd ed. (Cambridge University Press, 2006).
23. C. Y. Liu, S. Yuan, J. R. Dong, and S. J. Chua, "Temperature dependence of photoluminescence intensity from AlGaInP/GaInP multi-quantum well laser structures," J. Cryst. Growth **268**, 426–431 (2004).
24. J. J. D. Mckendry, D. Massoubre, S. Zhang, B. R. Rae, R. P. Green, E. Gu, R. K. Henderson, A. E. Kelly, and M. D. Dawson, "Visible-Light Communications Using a CMOS-Controlled Micro-Light-Emitting-Diode Array," J. Light. Technol. **30**, 61–67 (2012).
25. E. F. Schubert, "Light Emitting Diodes and Solid-State Lighting Solid-state lighting," (n.d.).
26. R. P. Green, J. J. D. McKendry, D. Massoubre, E. Gu, M. D. Dawson, and A. E. Kelly, "Modulation bandwidth studies of recombination processes in blue and green InGaN quantum well micro-light-emitting diodes," Appl. Phys. Lett. **102**, 091103 (2013).
27. S. Watson, M. Tan, S. P. Najda, P. Perlin, M. Leszczynski, G. Targowski, S. Grzanka, and a E. Kelly, "Visible light communications using a directly modulated 422 nm GaN laser diode.," Opt. Lett. **38**, 3792–4 (2013).
28. C. Lee, C. Zhang, M. Cantore, R. M. Farrell, S. H. Oh, T. Margalith, J. S. Speck, S. Nakamura, J. E. Bowers, and S. P. DenBaars, "4 Gbps direct modulation of 450 nm GaN laser for high-speed visible light communication," Opt. Express **23**, 16232 (2015).
29. S. Randel, F. Breyer, S. C. J. Lee, and J. W. Walewski, "Advanced modulation schemes for short-range optical communications," IEEE J. Sel. Top. Quantum Electron. **16**, 1280–1289 (2010).
30. S. Loquai, R. Kruglov, B. Schmauss, C. Bunge, F. Winkler, O. Ziemann, E. Hartl, and T. Kupfer, "Comparison of Modulation Schemes for 10. 7 Gb/s Transmission Over Large-Core 1 mm PMMA Polymer Optical Fiber," J. Light. Technol. **31**, 2170–2176 (2013).
31. G. Stepniak, L. Maksymiuk, and J. Siuzdak, "Experimental Comparison of PAM, CAP, and DMT Modulations in Phosphorescent White LED Transmission Link," IEEE Photonics J. **7**, 1–8 (2015).

1. Introduction

Solid-state visible light sources based on the InAlGaN material systems have become key enablers for a number of applications including lighting and illumination [1], displays [2], and

consumer electronics [3]. For example, InGaN-based white light emitting diodes (WLEDs) are replacing older light bulb technologies for home and street illuminations while InGaN laser diodes are at the core of blue-ray disc readers and are being considered for future ultra-efficient lighting [4]. An emerging application, visible light communications (VLC), has also been gathering a lot of attention recently [5]. Because practical InGaN optoelectronic sources do not yet cover the entire visible spectrum (efficiency drops continuously for wavelengths above 500 nm [6]), a blue GaN source often needs to be combined with color-converting materials to access longer wavelengths. This is usually done with rare-earth phosphors, as in commercial white LEDs [7]. However, phosphors respond slowly to modulated light, which is not ideal for VLC. Other color-converting materials are therefore being researched for VLC including organic semiconductors [8,9], colloidal nanocrystals [10] and inorganic semiconductor epilayers [11]. The latter offers an all-inorganic, photostable solution to color-conversion, which is particularly attractive for high power applications.

Recently, we have demonstrated a hybrid green-emitting LED based on a II-VI multi-quantum well (MQW) epilayer structure a couple of micron-thick for color-conversion of a blue LED [8]. Other groups had previously shown similar heterogeneous hybridization of epitaxial structures as a way to push the emission of GaN LEDs to longer wavelengths [9, 10]. In this work, we report the implementation of a red-emitting AlInGaP semiconductor color-converting structure and demonstrate free space VLC when it is combined with blue InGaN sources. The AlInGaP structure is a nanomembrane (NM, thickness below 400 nm) comprising a multi-quantum well active region. The NM format facilitates the heterogeneous integration of the color-converter with other materials and structures through capillary bonding. We focus on a device implementation where the AlInGaP NM is fully integrated with a micro-LED array. The result is an array of hybrid red LEDs that benefits from the relatively high modulation bandwidth of the underlying blue micro-LEDs [14]. Additionally, we demonstrate a proof-of-principle format for remote pumping with a blue laser diode where the NM is simply bonded onto a hemispherical sapphire lens. In both implementations, VLC experiments are done by modulating the GaN-based source with the modulated blue light being transferred to red by radiative down-conversion through the NM.

The rest of the paper is organized as follows: section 2 describes the design of the AlInGaP NM and its integration with the micro-LED array and/or the hemispherical sapphire lens. A description of the micro-LED array and the characterization methods are also given. Sections 3 and 4 report and discuss, respectively, the continuous-wave (CW) characteristics of the NM-based sources, and their dynamic and the VLC performance under *M*-ary pulse amplitude modulation (M-PAM) and orthogonal frequency-division multiplexing (OFDM) modulation schemes.

2. Device fabrication and characterization

2.1 Design and fabrication

The color-converter structure is based on epitaxial AlInGaP grown on GaAs substrate by molecular beam epitaxy. The active region is made of 3 pairs of GaInP quantum wells, with AlGaInP as the barrier material, designed for a room temperature emission of 648 nm. The 2λ length of the MQW region (excluding the GaAs buffer) is chosen so that the finalized NM absorbs >90% of light at 450 nm. To obtain the NM, the GaAs substrate is removed by wet etching using a solution of H_3PO_4:H_2O_2:H_2O at a ratio of 3:4:3. The resulting NM has a thickness of <400 nm, and a typical surface area of a few mm^2.

In the first device implementation (hybrid LED), the NM is capillary-bonded using deionized water [15] onto the sapphire window of the micro-LED chip (Fig. 1(a)). A 2mm diameter sapphire hemispherical lens with a refractive index of 1.7 is in turn capillary-bonded on top of the NM to finalize the hybrid device (Fig. 1(b)). The micro-LED chip, with peak emission at 450 nm, is fabricated using a commercial p-*i*-n GaN structure grown on *c*-plane

sapphire, following the procedure reported in [16]. The chip is made of 8 micro-LED pixels of 4 different sizes, 50 x 50 μm^2, 75 x 75 μm^2, 100 x 100 μm^2 and 150 x 150 μm^2. It is mounted onto a printed circuit board and wire bonded to metal tracks connected to SMA connectors, in such a way that each pixel from the micro-LED array can be individually addressed. Fig. 1(c) presents a photoluminescence spectrum from the NM with a photograph as inset of the hybrid device under current injection with the color-converted light visible in the center.

In the second NM implementation, for the laser diode (LD) pumping embodiment, the NM is simply bonded to a sapphire hemispherical lens as depicted in Fig. 1(d). The other side of the membrane is optionally placed in contact with a distributed feedback reflector. The 450nm LD (OSRAM PL450B) pump is mounted in a Peltier-cooled metallic mount kept at a constant temperature of 25^0C.

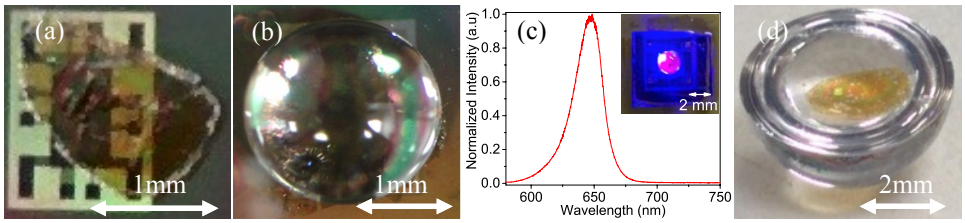

Fig. 1. MQW NM a) capillary bonded onto the sapphire window of the micro-LED chip, b) sandwiched in-between the sapphire hemispherical lens and the micro-LED window c) spectrum with a picture in inset from the hybrid LED with integrated sapphire lens under operation and d) capillary bonded onto the sapphire hemispherical lens for LD pumping.

2.2 Experimental methods

For reference, the different sizes of stand-alone blue micro-LEDs as well as the 450nm LD were first characterized, independently of the NM, in terms of optical power, emission spectrum and modulation bandwidths. The same measurements were then done with the AlInGaP NM (integrated with the micro-LEDs or remotely excited for LD pumping).

A set of aspheric lenses with focal length of 32 mm and high numerical aperture (NA of 0.612) were used to collect and focus the emission into a Femto HSA-X-S-1G4-SI photoreceiver (bandwidth of 1.4 GHz). For bandwidth measurements, the micro-LED or LD was simultaneously driven with a dc bias current and a frequency-swept modulated signal (0.250 Vpp) that were combined through a wideband (0.1–6000 MHz) Bias-Tee. An Agilent HP 8753ES Network Analyser was used to provide the modulation signal and to record the device frequency response as detected by the photoreceiver. A long-pass filter (550 nm cut-off wavelength) was placed before the receiver for measurements of the down-converted light. The modulation bandwidth was extracted from the detected modulation amplitude versus frequency as detailed in [9, 14]. The optical spectra were recorded with an Ocean Optics USB4000 Fiber Optic Spectrometer (2.5 nm resolution).

A similar set-up was used for the VLC demonstrations of section 4, with some specifics described here. For both PAM and OFDM, the modulated signal was generated offline in Matlab environment and load to an Agilent 81150A arbitrary waveform generator (AWG) while the detection was carried out by an 1.95mm diameter avalanche photodiode (APD) connected to an Agilent MSO71043 oscilloscope [18]. The post processing optical signal was done offline using a Matlab script. More information regarding the APD receiver and the OFDM test configuration can be found elsewhere [18,19].

3. CW characteristics

The curves of optical power versus drive current for the standalone micro-LEDs are plotted in Fig. 2(a). The slope is non-linear with the current and the curves eventually roll over at the highest currents. The smaller size micro-LEDs have a roll-over point at lower driving currents because they reach higher current densities for the same drive current. This non-linear behavior with the power roll over can be ascribed to an increase of the device temperature under operation, exacerbated by the phenomenon of efficiency droop [20,21]. The temperature rise can be related to the spectral shift of the emission as illustrated in Fig. 2(b) in the case of the 100 μm LED (black squares).

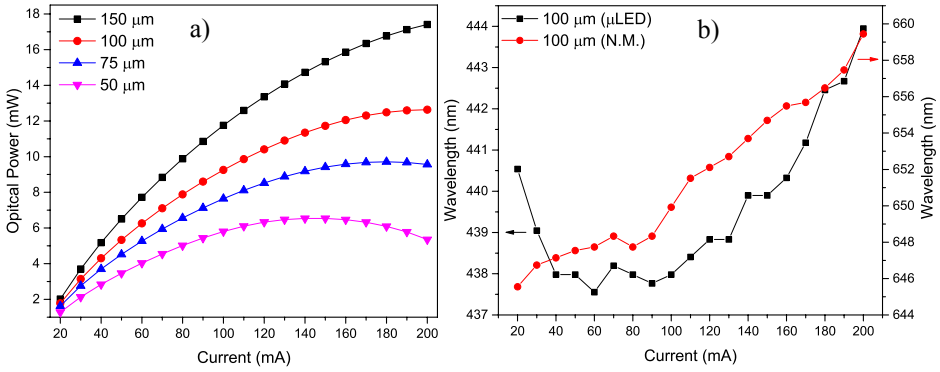

Fig. 2. a) L-I curve for each pixel in the μLED chip and b) spectral shift for the 100μm pixel and the III-V NM.

The emission from the micro-LED experiences an overall redshift of 3 nm, 441±1 nm and 444±1 nm, respectively, at 20 mA and 200 mA. The LED peak emission wavelength starts blue-shifting at lower current before reaching a plateau (60 mA – 100 mA) and eventually red-shifting for current above 100 mA. The initial blue shift is attributed to band filling and carrier screening of piezoelectric fields in the active region. At higher current injection the reduction of the bandgap energy with temperature becomes the predominant effect, resulting in the red shift [22]. The device increase in temperature under bias current was verified through thermal imaging of the sapphire substrate of the micro-LEDs. It was found that the temperature surface of the sapphire increases by approximately 140^0C between 20 and 200 mA.

Fig 3(a) plots the optical power versus current for the hybrid micro-LEDs (650nm emission). The trend is similar, with the biggest emitters giving the highest optical power, but the roll-over effect is more pronounced than for the stand alone micro-LEDs. For example, the 100μm stand-alone LED has a roll-over point between 180 and 200 mA whereas the equivalent hybrid LEDs rolls over at 100 mA. At this current the forward power conversion efficiency (i.e. the measured power of the red hybrid LEDs divided by that of the standalone blue micro-LEDs) is close to 1.2%. The efficiency decreases continuously for higher current. This decrease is attributed to a reduction of the NM luminescence efficiency as its temperature increases, the NM being in contact with the sapphire substrate. The peak emission wavelength of this hybrid micro-LED as a function of the drive current is also plotted in Fig. 2(b) (red dots). Unlike the blue micro-LED emission, the spectrum continuously red-shifts, going from 645 nm at 20 mA up to 658 nm at 200 mA. The spectral emission of the AlInGaP NM is expected to redshift by approximately 0.12 nm/C as determined from modeling based on the empirical Varshny relation [23]. Therefore the temperature increase of the NM can be inferred to be 100°C, which is not far off the temperature rise of the sapphire surface as measured by thermal imaging (140°C).

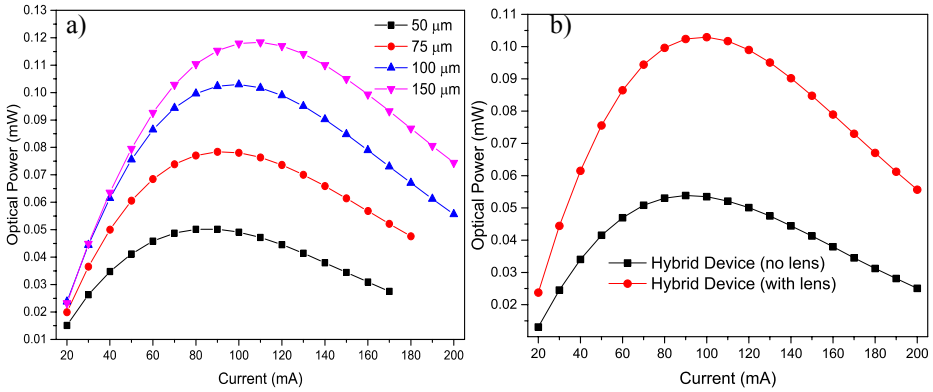

Fig. 3.a) L-I curve for the NM being remotely pumped with the 100μm pixel and b) power enhancement by addition of the lens for the 100μm device.

The hemispherical lens added on top of the NM helps to increase the forward conversion efficiency as shown in Fig. 3(b) in the case of the 100μm device where the maximum output power doubles. The hemispherical lens mitigates the problem of waveguided light within the NM as well as increases the collection of photon close to the escape cone limit. It is found that the maximum output power is improved by 63%, 92%, 98% and 95% for the squared pixels with edge size of 150, 100, 75 and 50 μm respectively. The lower enhancement for the 150μm device is probably because it sits on the edge of the lens. The addition of the lens however did not significantly improve heat removal from the NM; the red shift of the NM emission with current, with and without the lens, was found to be basically identical. For better thermal management, bigger lenses as well as active heat extraction from the lens could be used. Lenses could also be made with materials of higher thermal conductivity such as diamond.

Above, the decrease in the NM luminescence efficiency is attributed to a rise in temperature solely. But other possible explanations could include a dependence of non-radiative recombination with the MQW carrier density or a saturation of the NM absorption. To rule out these possibilities, the power density dependence of the converted light was further studied independently of the temperature rise caused by the micro-LED by remotely pumping a NM bonded onto a sapphire lens in the LD excitation configuration (as shown in Fig. 1d). For low pump power density onto the NM, a micro-LED was used otherwise the LD was utilized. The size of the pump onto the NM surface, needed for determination of the pump power density, was measured using a beam profiler. Results plotted in Fig. 4 (black triangles) demonstrate that there is no saturation of the absorption and no noticeable increase in non-radiative recombination; the optical power from the NM increases linearly with the pump power density on a range of 0 up to 4 kW/cm^2. The left side of the broken x-axis are data under LED pumping whereas on the right side are data for LD pumping.

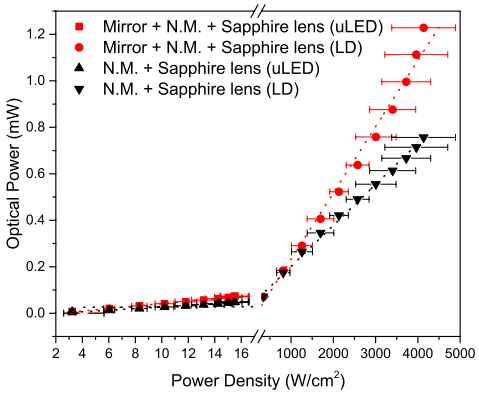

Fig. 4. Optical power vs power density for the NM bonded onto a sapphire lens and sandwiched between the sapphire lens and a dichroic mirror.

The converted power efficiency on this overall range is 0.88 ± 0.16%. The addition of a dichroic distributed feedback reflector, so that the NM is sandwiched between the lens and the mirror, increases the forward power efficiency to 1.14 ± 0.26% (red dots in Fig. 4), with an output power of 1.2 mW for a pump power density of 4 kW/cm^2.

4. Dynamic characteristics

4.1 Bandwidth measurements

The optical modulation bandwidth (the frequency at which the modulated optical power is half the dc value) versus drive current for the different sizes of stand-alone and hybrid micro-LEDs are plotted in Fig. 5(a) and 5(c) respectively. The intrinsic bandwidth of NM is plotted in Fig. 5(b).

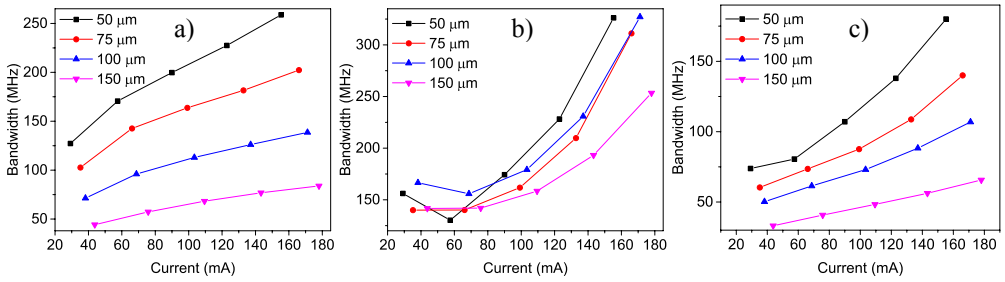

Fig. 5. Bandwidths for, a) each size of the stand-alone b) the NM and c) the hybrid micro-LEDs.

The bandwidth is size and current dependent reaching a maximum of 260 MHz and 180 MHz at around 150 mA for the standalone micro-LED and the hybrid red device respectively. The current dependency can be attributed to the reduced carrier lifetime in the active region of the micro-LEDs as the current, and hence the carrier density, increases [24]. The response of the NM further affects the bandwidth of the hybrid sources. The intrinsic response of the NM is between 130 MHz and 320 MHz, which is at least two order of magnitude faster than conventional phosphors [25,26]. The increase in the bandwidth with the current is linked to the increase of non-radiative recombination as the temperature of the device, hence of the NM, increases.

The frequency response of the LD could not be measured, as it was higher than the photodiode bandwidth of 1.4 GHz [27,28]. Even though, the NM bonded onto the sapphire lens bandwidth was measured and is shown in Fig. 6.

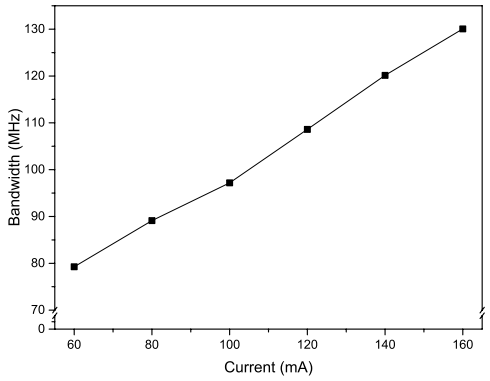

Fig. 6. Bandwidth from the LD-pumped NM-lens structure (line is a guide to the eye).

In Fig. 6 the bandwidth is set by the intrinsic response of the NM. There is a difference between the maximum achievable bandwidths, 180 MHz for the hybrid device and 130 MHz is for the LD-pumped NM. Again, this because of the increase of non-radiative recombination caused by heating when the NM is integrated onto the micro-LED array. When remotely-pumped heating is nowhere near as severe.

4.2 M-PAM and ODFM measurements

Free-space data transmission, using the NM device formats described above, was carried out. The optical set-up and the required equipment were described in section 2.2. Two modulation schemes were studied: PAM and OFDM. The optical and electrical conditions were kept identical between the different modulation tests. A pseudo random binary sequence (PRBS) of 10^{14}-1 was generated and encoded into appropriate PAM level, which are then loaded to Agilent 81180A AWG. A fractionally-spaced adaptive decision feedback equalizer (DFE) was adopted at the receiver. The DC-biased optical OFDM (DCO-OFDM) with bit and power loading algorithm was adopted for this work as in [19]. The OFDM signal conditioning including quadrature amplitude modulation (QAM) constellations mapping, an inverse fast Fourier transform (IFFT) and signal clipping were carried out offline. The conditioned discrete signal is supplied to the AWG. For DCO-OFDM, a FFT size of 512, cyclic prefix of 10 and clipping level of ±2.5 were adopted in this work. However, exhaustive searches for optimum parameters were not carried out.

The DCO-OFDM signal was then optically transmitted through free space by the source and detected by the APD.

The BER vs data rates for PAM and DCO-OFDM schemes for the hybrid micro-LEDs are presented in Fig. 7 and achieved data rates at BER of 3.8 $x10^{-3}$ is summarized in Table I. The best performing scheme under the experimental conditions is 4-PAM irrespective of micro-LED size. The smallest micro-LED offered the highest data rate for all modulation schemes due to higher bandwidth. Among PAM schemes, 4-PAM with DFE offered the best performance closely followed by 2-PAM. These results closely follows theoretical predictions in [29] where it is shown that 4-PAM requires less SNR than 2-PAM when data rate is beyond 5-times the electrical bandwidth. In comparison to PAM with DFE, the DCO-OFDM with bit and power loading does not offer advantage though the performance gap is smaller for larger size µLEDs. The OFDM offers advantage only when available SNR is very high (~30dB) so that data can be loaded much beyond the bandwidth [30,31]. Maximum SNR

obtained in this experiment were ~22dB. Another possible cause of inferior performance of OFDM is the system non-linearity cause by NM member and micro-LEDs, mitigation of which is not explored in this work.

Table 1 – Achievable data rates at BER of 3.8×10^{-3} for the different size of hybrid micro-LEDs in Mbit/s.

	50 x 50 μm^2	75 x 75 μm^2	100 x 100 μm^2	150 x 150 μm^2
2-PAM	777	757	738	659
4-PAM	867	862	807	615
8-PAM	720	740	680	495
OFDM	740	665	655	564

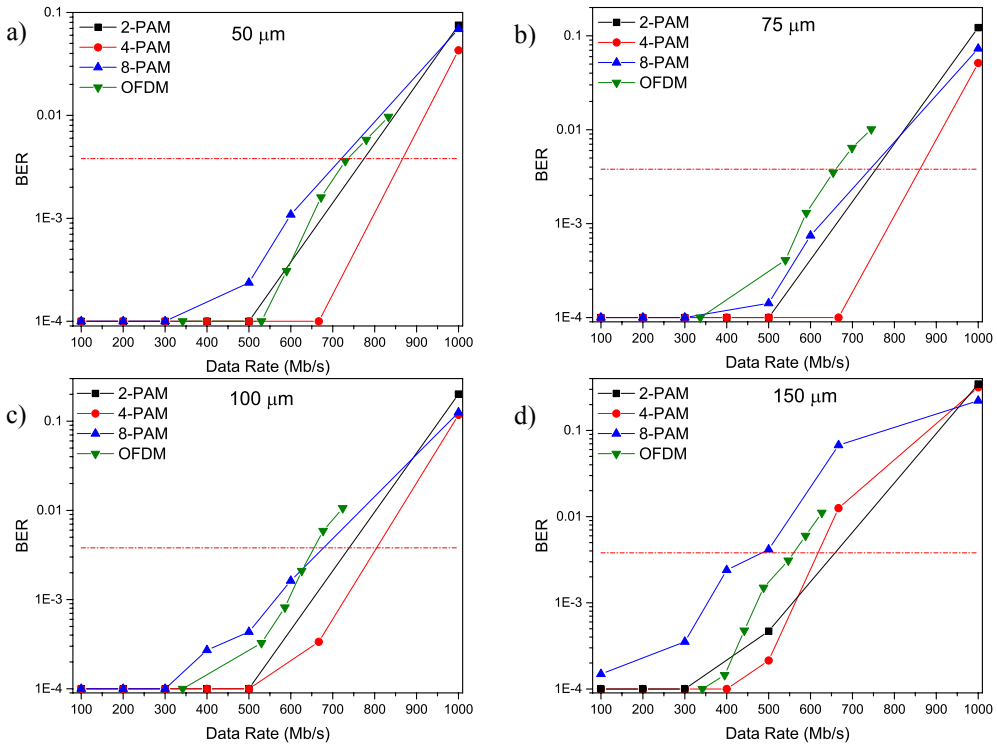

Fig. 7 – BER vs Data Rate for the hybrid devices a) 50μm x 50μm pixels, b) 75μm x 75μm pixels, c) 100 μm x 100μm pixels and d) 150μm x 150 μm pixels.

DCO-OFDM data transmission using the LD-pumped NM (Fig 1(d)) was also tested. By adjusting the LD driving bias current and the modulation depth, it was possible to achieve transmission up to 1.2 Gb/s at BER of 3.8×10^{-3} as shown in Fig. 8. The higher data rate is due to the combined higher SNR level and higher modulation bandwidth of the laser diode in comparison to the micro-LEDs.

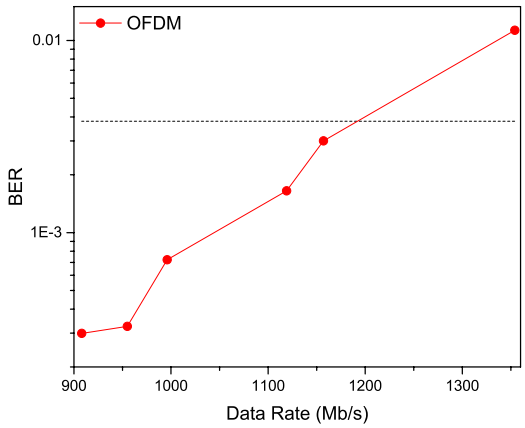

Fig. 8 - BER vs Data Rate for the sample pumped with a laser diode.

5. Conclusion

In this paper, we have demonstrated VLC using InGaN sources color-converted with AlInGaP NM assemblies. The NM geometry of the converter enables integration with optics and micro-LEDs by capillary bonding. A hybrid red-emitting micro-LED arrays, incorporating a sapphire lens, was thus demonstrated. The maximum data rate achieved for this hybrid configuration was 867 Mb/s using 4-PAM scheme. We also reported on a NM format for remote pumping by LD. In this configuration we have shown VLC up to 1.2 Gb/s using OFDM. This second configuration would be particularly suited for high power applications with the NM bonded to optics and heat spreaders. Finally, by designing other NM structures using AlGaInP or InGaN material systems it should be possible in principle to extend the wavelength coverage across the visible spectrum.

Acknowledgments

This research work was supported by the EPSRC Programme Grant “Ultra-parallel visible light communications (UP-VLC)” (EP/K00042X/1). The authors would like to acknowledge Dr. Enyuan Xie for the micro-LED fabrication.